Supplementary Information

Surfactant-coated iron oxide nanoparticles synthesized by coprecipitation as potential phosphate adsorbents in peritoneal dialysis

Théo Lucante[a,b], Anne Carton[a], Jan Niklas Schmidt[a], Céline Kiefer[a], Philippe Choquet[c-e], Ariane Zaloszyc[b,e,f], Sylvie Bégin-Colin[a,b*]

[a] *University of Strasbourg and CNRS, Institut de Physique et Chimie des Matériaux de Strasbourg, UMR 7504, 23 rue du Loess, 67034 Strasbourg Cedex 2, France*

[b] *University of Strasbourg and CNRS, Institut de Chimie et Procédés pour l'Énergie, l'Environnement et la Santé, UMR 7515, 25 rue Becquerel, 67087 Strasbourg, France*

[c] *University of Strasbourg and CNRS, Laboratoire des Sciences de l'Ingénieur, de l'Informatique et de l'Imagerie, UMR 7357*

[d] *Preclinical Imaging Lab, Imaging Dpt, Hôpitaux Universitaires de Strasbourg, Strasbourg, France*

[e] *University of Strasbourg, Faculté de Médecine, Maïeutique et Sciences de la Santé, Strasbourg, France*

[f] *Nephro-pediatry, CHU Hautepierre, Hopitaux Universitaire de Strasbourg, 1 avenue Molière, 67098 Strasbourg, France*

Table S1. Composition of the dialysate used in this work: BICAVERA 1.5 % Glucose, 1.75 mmol.L^{-1} Calcium, solution for peritoneal dialysis (Fresenius Medical Care, Germany).

Active substance	Mass concentration (g.L^{-1})	Species in solution	Molar concentration (mmol.L^{-1})
$CaCl_2.2H_2O$	0.2573	Ca^{2+}	1.75
NaCl	5.786	Na^+	134
$NaHCO_3$	2.940	Mg^{2+}	0.5
$MgCl_2.6H_2O$	0.1017	Cl^-	104.5
$C_6H_{12}O_6.H_2O$	16.5	HCO_3^-	34
Eq. $C_6H_{12}O_6$	15.0	$C_6H_{12}O_6$	83.25

SI.I. Post-synthesis coating of naked IONPs with the anionic surfactants

Protocols for the post-synthesis coating of naked IONPs with PAA and TA have been developed based notably on the works of Daou *et al.*[1] and Basly *et al.*[2]. Indeed, these works aimed at grafting dendron molecules bearing a phosphonate anchoring group at the surface of naked IONPs synthesized by coprecipitation. These previous grafting have been performed in acidic pH water, *i.e.* a pH value where electrostatic attractions are favored between the dendron's phosphate group (deprotonated, bearing a negative charge) and the iron oxide surface (protonated, conferring a positive ζ value to the IONPs). Indeed, IO surface possesses hydroxyl groups and Daou *et al.*[3] report that all Fe-OH sites are not equivalent and only ~20 % are amphoteric. At pH values below the IO IEP ($pH_{IEP} \approx 7$[4]), these surface groups are protonated giving a positive ζ to the IONPs. Above the IO IEP, these groups are deprotonated giving a negative ζ to the IONPs.

The same strategy is used here: coatings are performed at pH values intermediate between the IO IEP and the surfactant pK_a (PAA: pK_a = 4.3 – 4.5[5–7], TA: $pK_a \approx 6$[8]) for favoring electrostatic attractions between them (**Figure 2** in the main body of the article).

Step 1. First, the freshly synthesized naked IONPs are suspended in basic pH water (pH > 10). In a typical coating protocol, a suspension (10 mL) of IONPs (2 $mg.mL^{-1}$) in basic pH water is prepared. Its ϕ_{hydro} distribution is monomodal with a ϕ_{hydro} value of 161 ± 86 nm (PDI = 0.15) and a mean ζ value of -36 ± 1 mV (**Figure S1a,b**).

Step 1 → 2. Then, the suspension is placed in an ultrasound bath and its pH is quickly decreased to pH ≤ 2 using ~milliliters of a hydrochloric acid (HCl) solution (2 $mol.L^{-1}$) in order to limit nanoparticle aggregation when pH passes through the IO IEP. Sonication is continued for 15 min. There, the IONPs ϕ_{hydro} distribution stays monomodal with a ϕ_{hydro} value of 163 ± 84 nm (PDI = 0.16) and a positive ζ value of 35 ± 1 mV (**Figure S1a,b**). For this step, a nitric acid (HNO_3) solution (2 $mol.L^{-1}$) have also been used but the nanoparticle ϕ_{hydro} distribution, ϕ_{hydro} and ζ values are identical to those whose pH have been adjusted using HCl (**Figure S1c**). So, HCl has been used in all experiments. Also, it should be noted that the nanoparticle ζ value turns positive within 15 min only at pH ≤ 2: the ζ value stays negative at 2 < pH < IO IEP.

Step 2 → 3. The suspension pH is then carefully adjusted to 5 (for PAA coating) or 6 (for TA coating) using a sodium hydroxide (NaOH) solution (0.2 $mol.L^{-1}$) before 15 min in an ultrasound bath. There, the IONPs ϕ_{hydro} distributions stay monomodal with ϕ_{hydro} values of 205 ± 115 nm (PDI = 0.21, pH 5, **Figure S1a**) and 214 ± 117 nm (PDI = 0.23, pH 6, **Figure S1b**). For each suspension, approaching the IO IEP results in a slight increase in aggregation state, although their ζ value remains slightly positive: 17 ± 1 mV (pH 5) and 16 ± 1 mV (pH 6).

In parallel, PAA (0.113 $mg.mL^{-1}$) and TA (0.238 $mg.mL^{-1}$) solutions are prepared and their pH are adjusted to 5 or 6 respectively using a NaOH solution (0.2 $mol.L^{-1}$). With TA, this step requires to be particularly cautious since TA catechol groups are reported – and were observed in our previous work[9] – to undergo oxidation into quinones in mild alkaline conditions (*i.e.* pH ≥ ~8)[10–12], excessively lowering their adsorption on iron oxide surfaces[9,13–16].

Then, 10 mL of surfactant solution is added to the nanoparticle suspension and the mixture is mechanically stirred overnight. Using these volumes and concentrations, 1.13 mg (PAA) or 2.38 mg (TA) are in contact with 20 mg of naked IONPs, corresponding to the theoretical quantities required to form a surfactant monolayer on the nanoparticle surface. Indeed, the naked IONP SSA have been measured at 101 $m^2.g^{-1}$ by BET measurement (**Figure S1d**) while the geometrical cross section of one TA molecule is reported to be 2.4 nm^2 [17] (we approximate the PAA cross section to be also 2.4 nm^2).

Step 3 → 4. Finally, suspension pH is carefully adjusted to 7 with a NaOH solution. All the results on colloidal stability of suspensions at each step are summarized in **Table S2**.

However, PAA and TA post-coated IONPs did not display a good colloidal stability with time in both pH 7 water and dialysate. Colloidal stability of TA-coated IONPs has been tried to be improved using 10

times and 100 times the TA quantity required to form a monolayer on nanoparticles, but a significant sedimentation is still observed within 4 hours in pH 7 water, resulting in a very low yield of colloidally stable IONPs. Also, colloidal stability in dialysate is not improved.

Thus, electrostatic interactions would not be high enough to induce a strong anchoring of surfactant. In the case of TA-coated IONPs, various works report a poor colloidal stability over time for post-synthesis catechol-coated nanoparticles[13,14,18,19] and explain this by a sequential oxidation of catechol groups forming complexes with nanoparticle surface iron ions. Notably, Kim *et al.*[14] propose the following mechanism: first, catechol would form complexes with both surface Fe(II) and Fe(III). Then, an electron transfer would occur from catechol to Fe(III), forming an oxidized semiquinone and a reduced Fe(II). The so-formed semiquinone would then moves to an adjacent Fe(III) and oxidation would be repeated to form fully oxidized quinone detaching from the iron oxide surface since no anchor group is present anymore. Also, these works[14,20] propose adding electronegative groups to the catechol ring to enhance electronic interactions with iron oxides[18] and to prevent catechol oxidation into quinone[14]. Notably, they report a more stable catechol coating on iron oxide over time by adding an amine additive (AA) in the medium. They proposed that catechol and semiquinone could be recovered respectively from oxidized semiquinone and quinone through Michael addition of an AA, here the 2-(2-aminoethoxy) ethanol (AEE). In our work, some tests have been performed by adding AEE in the TA and nanoparticles mixture in pH 6 water before increasing the pH to 7, but without enhancing the nanoparticle colloidal stability.

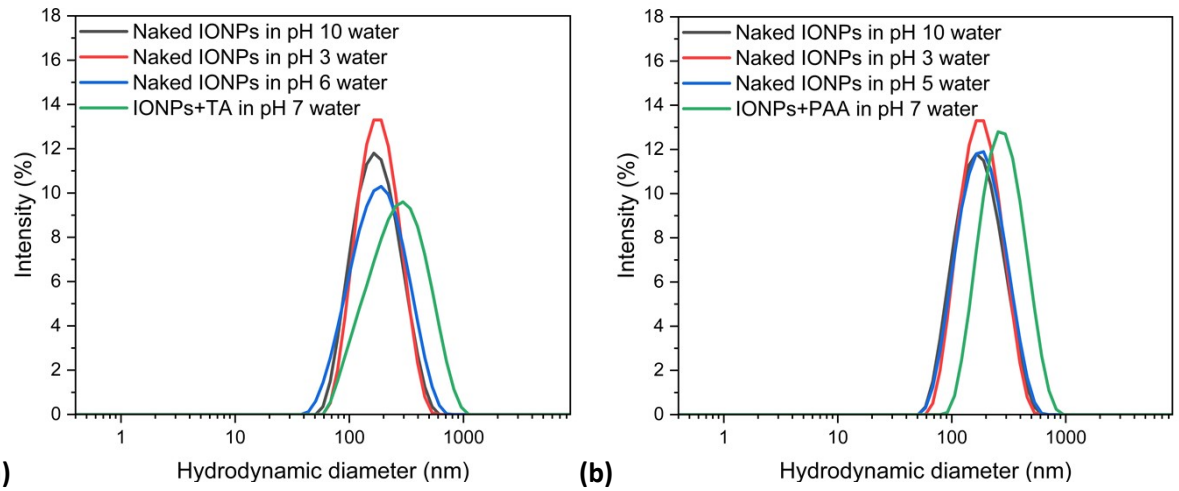

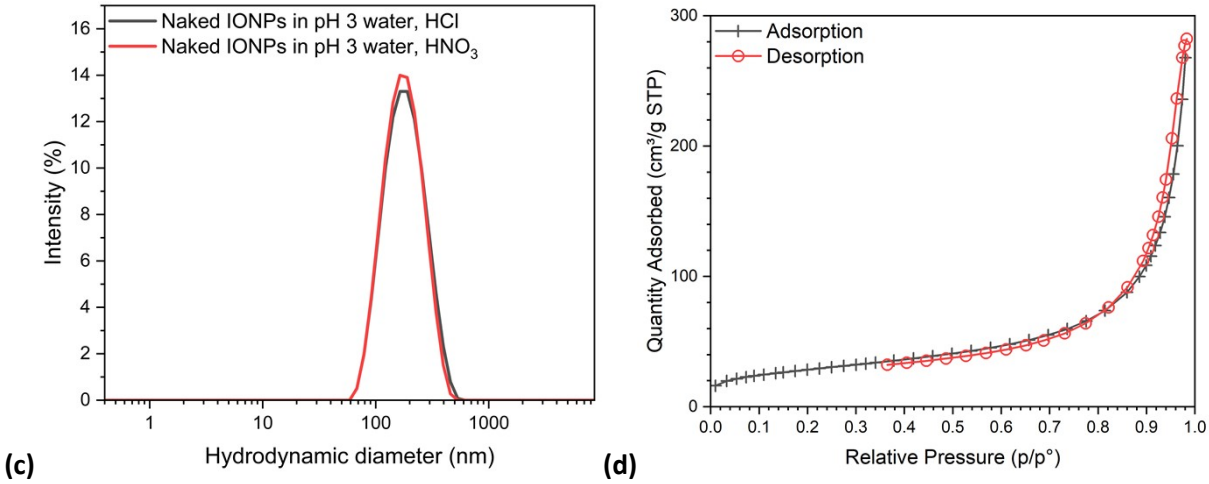

Figure S1. Hydrodynamic diameter distribution of **(a)** naked and post-synthesis PAA-coated IONPs along our coating protocol, **(b)** naked and post-synthesis TA-coated IONPs and **(c)** naked IONPs whose pH is adjusted from 10 to 2 using different acidic solutions. **(d)** BET curve of naked IONPs.

Table S2. Mean hydrodynamic diameter in intensity and mean zeta potential values of naked IONPs and post-synthesis surfactant-coated IONPs along our coating protocol.

	PAA			**TA**		
	ϕ_{hydro} (nm)	PDI	ζ (mV)	ϕ_{hydro} (nm)	PDI	ζ (mV)
Step 1	161 ± 86	0.15	-36 ± 1	161 ± 86	0.15	-36 ± 1
Step 1 → 2	163 ± 84	0.16	35 ± 1	163 ± 84	0.16	35 ± 1
Step 2 → 3	205 ± 115	0.21	17 ± 1	214 ± 117	0.23	16 ± 1
Step 3 → 4	310 ± 150	0.22	-44 ± 1	318 ± 186	0.23	-36 ± 1

SI.II. Optimization of the recovery time of anionic surfactant-coated IONPs

An important rate-determining step to be accelerated to produce enough PAA- and TA-coated IONPs is their size separation. Experimentally, suspensions recovered just after one-pot syntheses contain different sizes of IONPs aggregates, up to $\phi_{hydro} \geq 1000$ nm (**Figure S2a**). After one-week natural sedimentation, only one population of mean ϕ_{hydro} of 80 – 140 nm remains in suspension and is recovered (**Figure S2a**). This process is relatively slow because multiple forces are applied on IONPs in suspension, mitigating the gravitational force responsible for sedimentation, notably the drag force, the buoyancy force and the thermal fluctuation forces (Brownian motion)[21].

Among the various protocols reported in the literature, magnetic separation is particularly adapted for accelerating this step while maintaining a high nanoparticle yield. Indeed, it is known that superparamagnetic nanoparticles combined into aggregates increase their overall magnetic moment, which is the sum of the moments of all individual nanoparticles[22]. As a result, the magnetic response of larger aggregates to an external magnetic field is increased compared to small aggregates or individual nanoparticles[22]. In addition, larger aggregates have a lower diffusion coefficient, simplifying their magnetic recovery since the Brownian motion highly contributes to colloidal stability[22,23].

Just after their synthesis in one-pot, IONP@PAA and IONP@TA suspensions are diluted in 400 mL of distilled water in a 500 mL-capacity bottle (width = 8 cm, height from bottom to suspension water line ≈ 8.5 cm) then placed on a neodymium magnet (1.2 T). Then, their ϕ_{hydro} distribution is measured over time. In **Figure S2a**, the IONPs@TA ϕ_{hydro} distribution evolve towards a monomodal and moderately polydisperse distribution with a final ϕ_{hydro} value of 136 ± 59 nm (PDI = 0.19) after 4 days. In comparison, a monomodal distribution with similar ϕ_{hydro} (135 ± 68 nm, PDI = 0.22) is reached after 1-week natural sedimentation (**Figure S2b**). Also, continuing this magnetic separation process beyond 4 days do not further decrease the nanoparticle ϕ_{hydro}.

This protocol has also been used with IONPs@PAA and allowed us to obtain a monomodal distribution of ϕ_{hydro} = 100 ± 26 nm, PDI = 0.19 (*i.e.* slightly larger than after one-week sedimentation: ϕ_{hydro} = 81 ± 36 nm, PDI = 0.16) after 2 days magnetic separation (**Figure S2b**).

Thus, this protocol using magnetic sedimentation allowed us to accelerate the nanoaggregate size separation step and obtain suspensions with monomodal distribution, suitable ϕ_{hydro} value and high colloidal stability in only 4 days (IONPs@TA) or 2 days (IONPs@PAA) instead of 1-week natural sedimentation.

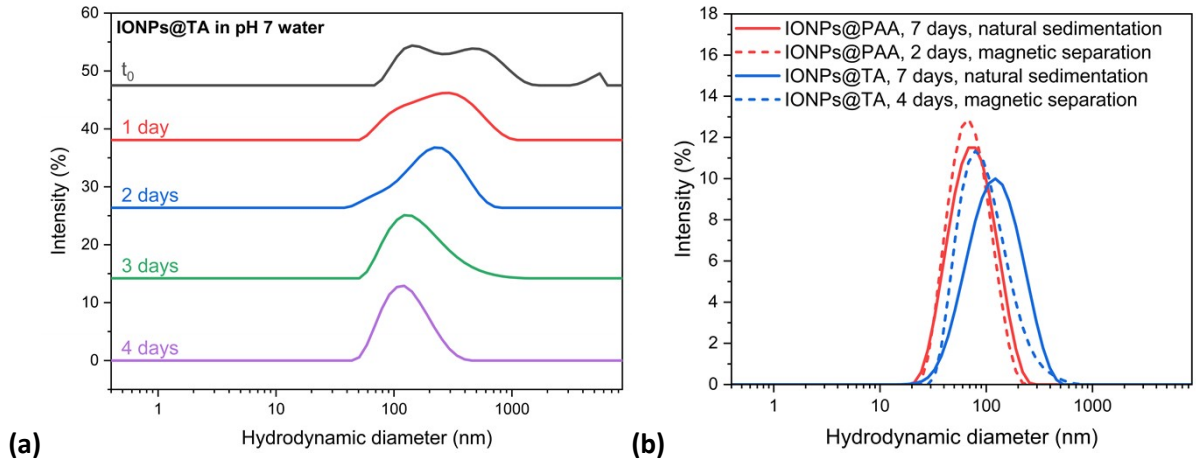

Figure S2. Hydrodynamic diameter distribution of **(a)** IONPs@TA in pH 7 water over time performing magnetic separation and **(b)** of IONPs@PAA and IONPs@TA in pH 7 water after 1-week natural sedimentation and 2 days (IONPs@PAA) or 4 days (IONPs@TA) magnetic separation.

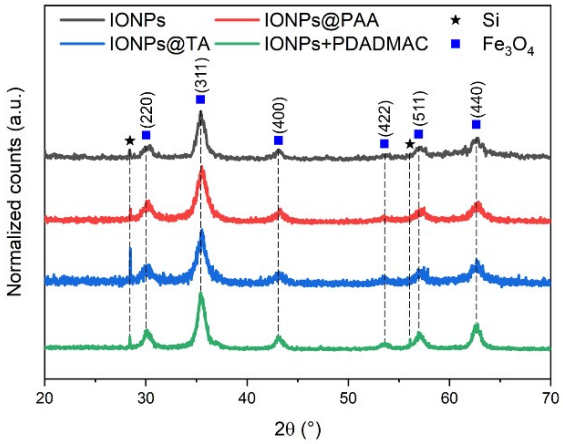

Figure S3. XRD pattern of naked IONPs and surfactant-coated IONPs.

SI.III. Analysis of FTIR spectra of surfactant-coated IONPs

Surfactant presence on IONPs have been first investigated by FTIR spectroscopy. In **Figure S4a**, each nanoparticle exhibit a Fe-O band localized at 594 cm^{-1} (IONPs@PAA), 592 cm^{-1} (IONPs@TA) and 584 cm^{-1} (IONPs+PDADMAC). In each case, the Fe-O band possesses a broad shoulder towards the high wavenumbers, which is characteristic of an oxidized magnetite phase[9,24,25]. Indeed, the IR spectrum of non-oxidized magnetite displays one Fe-O band at ~580 cm^{-1} while that of maghemite exhibits several bands in the wavenumber range 800 – 400 cm^{-1} and whose resolution depends on the ordering of vacancies in maghemite[25].

Compared to the naked IONPs spectrum, a new band at 1727 cm^{-1} appears on the IONPs@PAA spectrum (**Figure S4b**) and is attributed to the stretching mode of the PAA C=O bond, which has been shifted from 1710 cm^{-1} in the PAA spectrum (**Figure S4a**). Similarly, a new band at 1455 cm^{-1} is assigned to the in-plane bending mode of CH_2 bond located at 1454 cm^{-1} in the PAA spectrum[26,27]. Furthermore, two very broad bands at 1406 cm^{-1} and 1577 cm^{-1} would contain the symmetrical (ν_s) and asymmetrical (ν_{as}) stretching vibration modes of the COO^- bond[26,28] respectively. As discussed in the main body of the article, the PAA carboxylate groups can interact with iron oxide surfaces to form different types of complexes and in the literature, analyzing the separation between ν_{as} and ν_s bonds may allow identifying which type of complex is on surface[26,28,29]. However, a HRTEM image (**Figure 3f** in the main body of the article) shows multiple layers around our IONPs@PAA. Therefore, PAA in IONPs@PAA is expected not only to form complexes with the iron oxide surface, but also having free deprotonated carboxylate and carboxyl groups whose contributions are included in the broad bands at 1406 cm^{-1} and 1577 cm^{-1}. It is therefore difficult to identify which complex is formed on the iron oxide surface. Complete band attribution in PAA and IONPs@PAA spectra is detailed in **Table S3**.

Then, the IONPs@TA spectrum (**Figure S4c**) displays new TA bands compared to that of naked IONPs, and are identified according to our previous work (characterization of TA-coated iron oxide nanoclusters synthesized in a one-pot polyol solvothermal synthesis)[9]. The broad band at 1585 – 1619 cm^{-1} is attributed to the stretching of aromatic C-C bonds in TA (in TA spectrum: 1614 cm^{-1}) while the new bands at 1198 cm^{-1} and 1049 – 1098 cm^{-1} are assigned to bonds from the phenolic groups of TA[9,30], *i.e.* symmetrical stretching of C-O-C (in TA spectrum: 1085 cm^{-1}), stretching of O-CO and C_{ar}-CO and in-plane bending of C_{ar}-O-H at 1196 cm^{-1} despite the band shape modifications[9,31,32]. In addition, the new TA band at 1363 cm^{-1} would be characteristic of the complex formed by TA on iron oxide surface[9]. Similar to the spectrum of TA-coated iron oxide nanoclusters in our previous work[9], the C=O band at 1717 cm^{-1} attributed to phenolic ester in TA disappears in IONPs@TA spectrum. This has been proposed to be due to organisation and interactions of TA molecules on the iron oxide surface or between multiple TA molecules coating the iron oxide surface[9]. Also, it should be noted that a band at 948 cm^{-1} attributed to the skeletal vibration of tetramethylammonium ions $N(CH_3)_4^+$ is still present in IONPs@TA spectrum even if more than three washes by an ultrafiltration protocol are performed (see **Section 4.2.2** in the main body of the article). A proposal of IR band attribution in TA and IONPs@TA spectra is given in **Table S3**.

Finally, in **Figure S4d**, the FTIR spectrum of IONPs+PDADMAC showed little evidence of the surfactant presence, with only one new band located at 1467 cm^{-1} and previously attributed to the in-plane

bending mode of CH_2 bond. Thus, FTIR spectroscopy alone is unable to confirm the presence of the cationic surfactant, suggesting a purely physical adsorption of PDADMAC on the iron oxide surface. This would be consistent since PDADMAC does not have any anchoring group for the iron oxide surface and therefore cannot form covalent bonds with the surface hydroxyl groups. IR band attribution in PDADMAC and IONPs+PDADMAC spectra is proposed in **Table S3**.

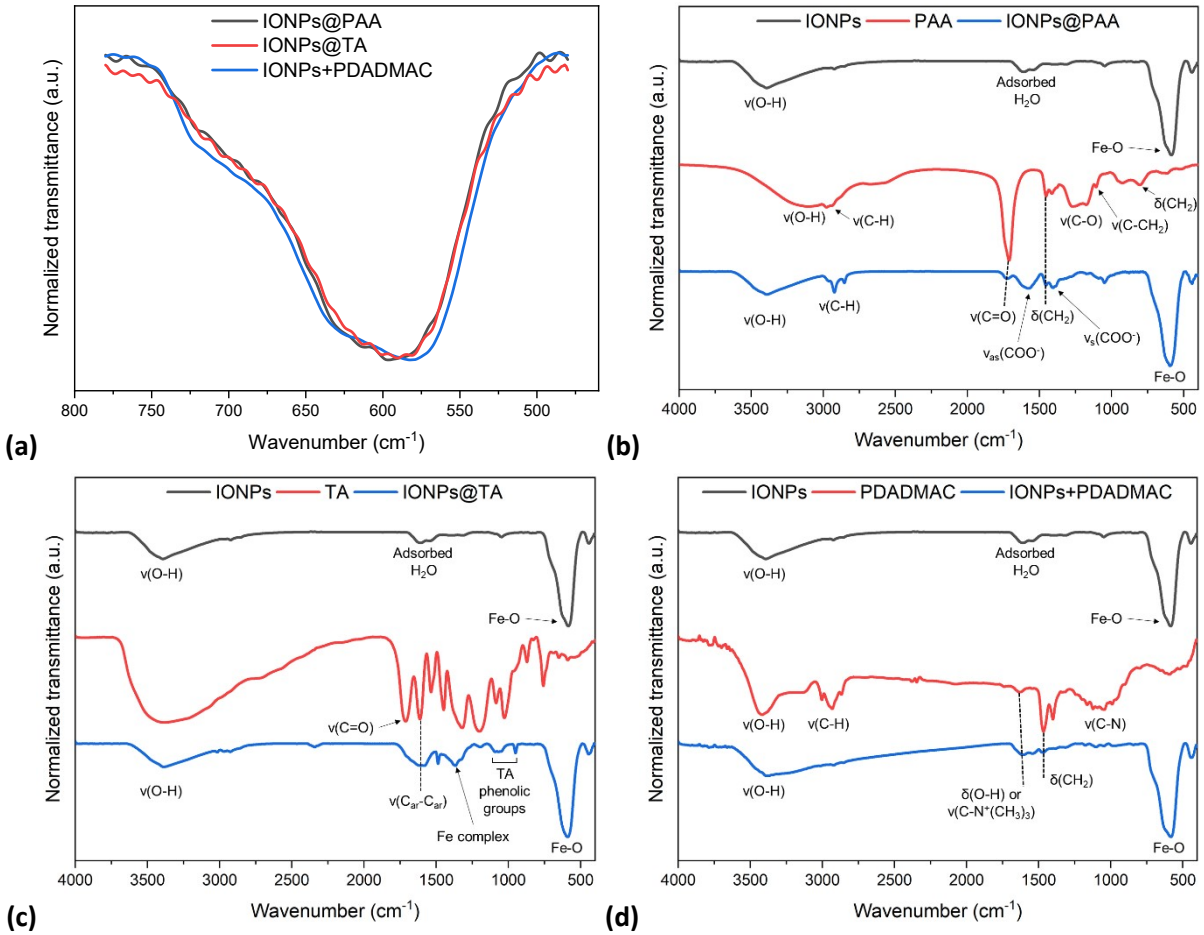

Figure S4. Superimposed FTIR spectra of the surfactant-coated IONPs in the region of the Fe-O vibration band of iron oxide. FTIR spectra of **(b)** IONPs, PAA and IONPs@PAA; **(c)** IONPs, TA and IONPs@TA and **(d)** IONPs, PDADMAC and IONPs+PDADMAC. v, stretching; δ, bending.

Table S3. Proposal for band attribution in IONPs@PAA, IONs@TA and IONs+PDADMAC FTIR spectra and the associated surfactants.

PAA	**IONPs@PAA**	
Wavenumber (cm^{-1})	Wavenumber (cm^{-1})	Attribution[26–28,33]
2937 – 2975m	2852 – 2922m	CH_2 or CH stretching
1710vs	1727w	C=O stretching
-	1577m	Contains COO^- asymmetric stretching
1454m	1455w	CH_2 bending
1415m	-	C-O stretching and O-H bending
-	1406m	Contains COO^- symmetric stretching
1180 – 1270s	-	C-O stretching and O-H bending
1104w	-	C-CH_2 stretching
927w	-	O-H bending
805w	-	CH_2 bending and C-COOH stretching
-	594vs	Fe-O
TA	**IONPs@TA**	
Wavenumber (cm^{-1})	Wavenumber (cm^{-1})	Attribution[9,30–32,34]
1717s	-	C=O stretching (phenolic ester)
1614s	1585 – 1619m	C-C stretching (aromatic), H_2O (IONPs@TA)
1535m	-	Ring stretching, C-OH bending, C-H bending
-	1488m	CH_3 asymmetric deformation ($N(CH_3)_4^+$)
1448s	-	C=C stretching (aromatic), O-H stretching
-	1363m	Iron complex
1320s	-	C_{ar}-O-C stretching, C_{ar}-O-H bending
-	1198m	Phenolic groups of TA
1196s	-	O-CO stretching, C_{ar}-CO stretching, C_{ar}-O-H bending
1085m	-	C-O-C symmetric stretching (aryl phenolic ester)
-	1049 – 1098w	Phenolic groups of TA
1027m	-	C-O asymmetric stretching
960w, sh	-	C-COOH stretching
-	948m	$N(CH_3)_4^+$ skeletal vibration
870w	-	O-H bending, C-H bending
828 w	-	C-H bending (aromatic)
758w	-	C-H and O-H bending
-	592vs	Fe-O
PDADMAC	**IONPs+PDADMAC**	
Wavenumber (cm^{-1})	Wavenumber (cm^{-1})	Attribution[35–37]
2865 – 3007s	-	CH_2 stretching
1630w	1613w	O-H bending or C-$N^+(CH_3)_3$ stretching
1467s	1467w	CH_2 bending
1040 – 1124s	-	C-N stretching
-	584vs	Fe-O

vs, very strong; s, strong; m, medium; w, weak; sh, shoulder.

SI.IV. Analysis of TGA curves of surfactant-coated IONPs

TGA under air have been performed to confirm the presence and quantify the surfactants on each nanoparticle. The results are presented in **Figure S5**. For IO-CP@PAA, TGA and DTG curves show two main thermal phenomena starting at ~150 °C and ~240 °C respectively, with DTG maxima at ~200 °C and ~280 °C. The final weight loss at 800°C is ~49 %. In the literature, a multi-step thermal degradation of PAA is often reported (with a first thermal event above 200 °C) attributed to dehydration of carboxylic groups, to decarboxylation and/or to chain scission[38]. Our IONPs@PAA TGA/DTG curves display similar events so the first one starting at ~150 °C is attributed to dehydration of adsorbed and hydrogen-bonded water molecules on iron oxide surface while the second is attributed to PAA decarboxylation and degradation[39,40]. Hayashi *et al.*[39] also reported a third event at ~600 °C but it is not observed with our IONPs@PAA.

TGA/DTG curves of IONPs@TA display one thermal event starting at 180 °C (DTG maximum at ~280 °C) and the final weight loss at 800 °C is 58 %. Such a main DTG peak between 250 – 300 °C have already been observed in a previous work[9] for iron oxide nanoclusters coated with the highest TA-loading studied, and have been attributed to the decomposition of TA.

Finally, multiple thermal events are identified in the TGA/DTG curves of IONPs+PDADMAC: at ~210 °C, ~405 °C and ~635 °C with DTG maxima at ~330 °C, ~450 °C and ~665 °C respectively. The final weight loss at 800 °C is 66 %. These results are in accordance with the work of Francis *et al.*[41], where a first event with maximum DTG at 320 °C have been attributed to quaternary ammonium dissociation with the formation of alkyl halide while a second event with maximum DTG at 453 °C have been observed but not attributed to a specific PDADMAC decomposition mechanism.

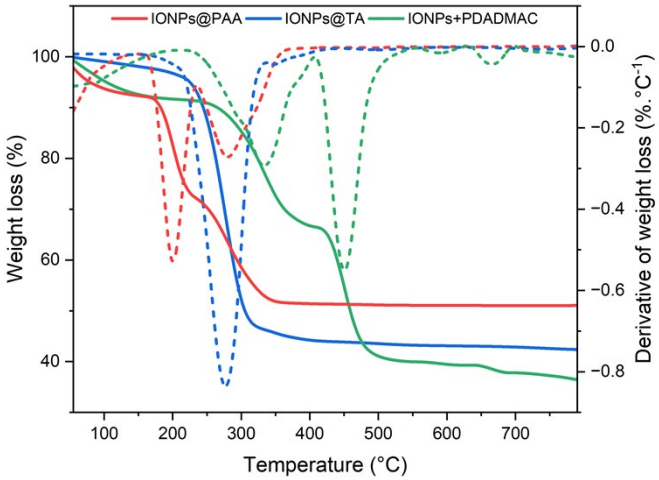

Figure S5. TGA (solid lines) and DTG curves (dotted lines) of each surfactant-coated nanoparticle.

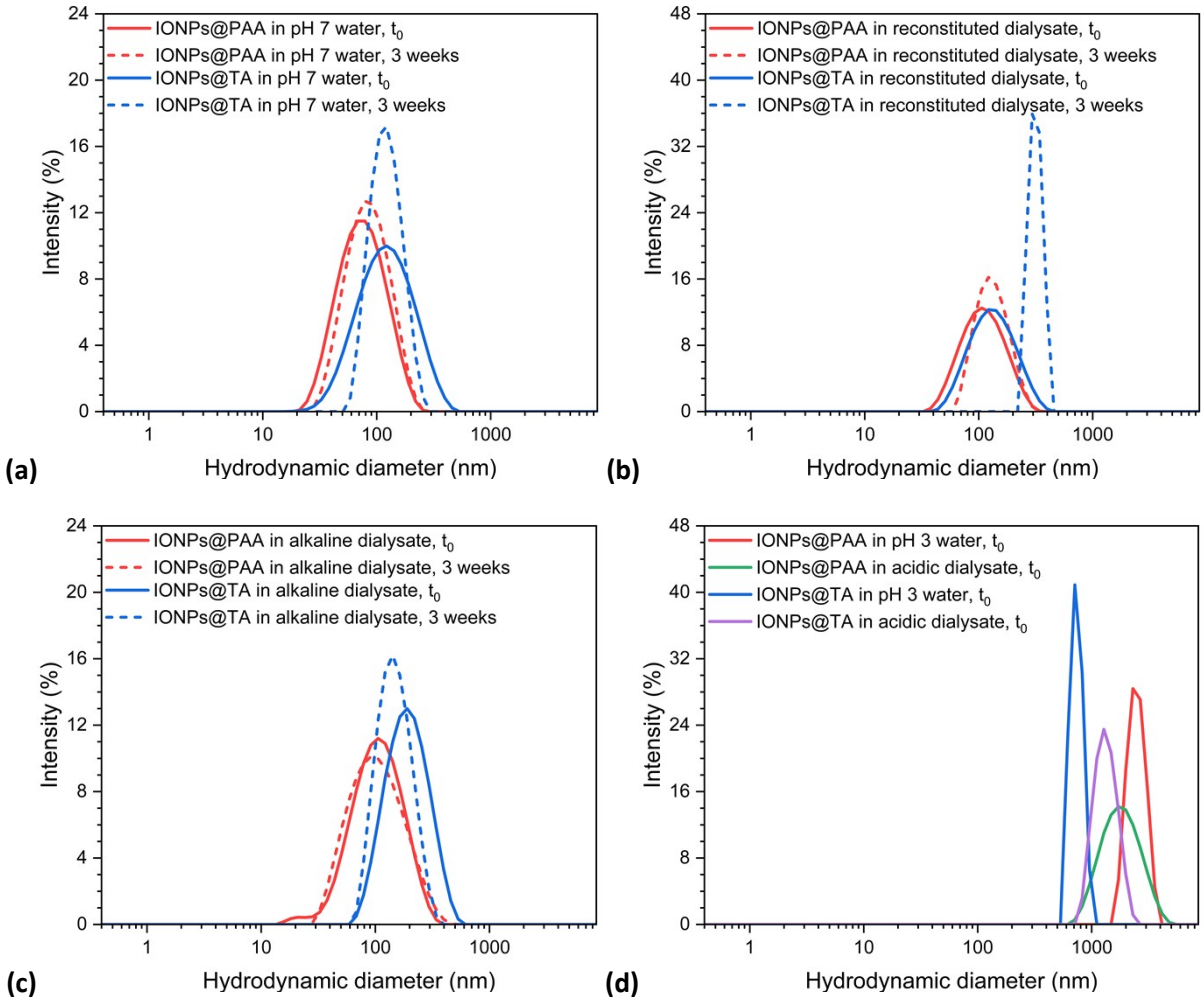

Figure S6. Hydrodynamic diameter distributions of PAA- and TA-coated IONPs at t_0 and after three weeks in **(a)** pH 7 water, **(b)** reconstituted dialysate and **(c)** alkaline dialysate. **(d)** IONPs@PAA and IONPs@TA hydrodynamic diameter distributions at t_0 in ph3 water and acidic dialysate.

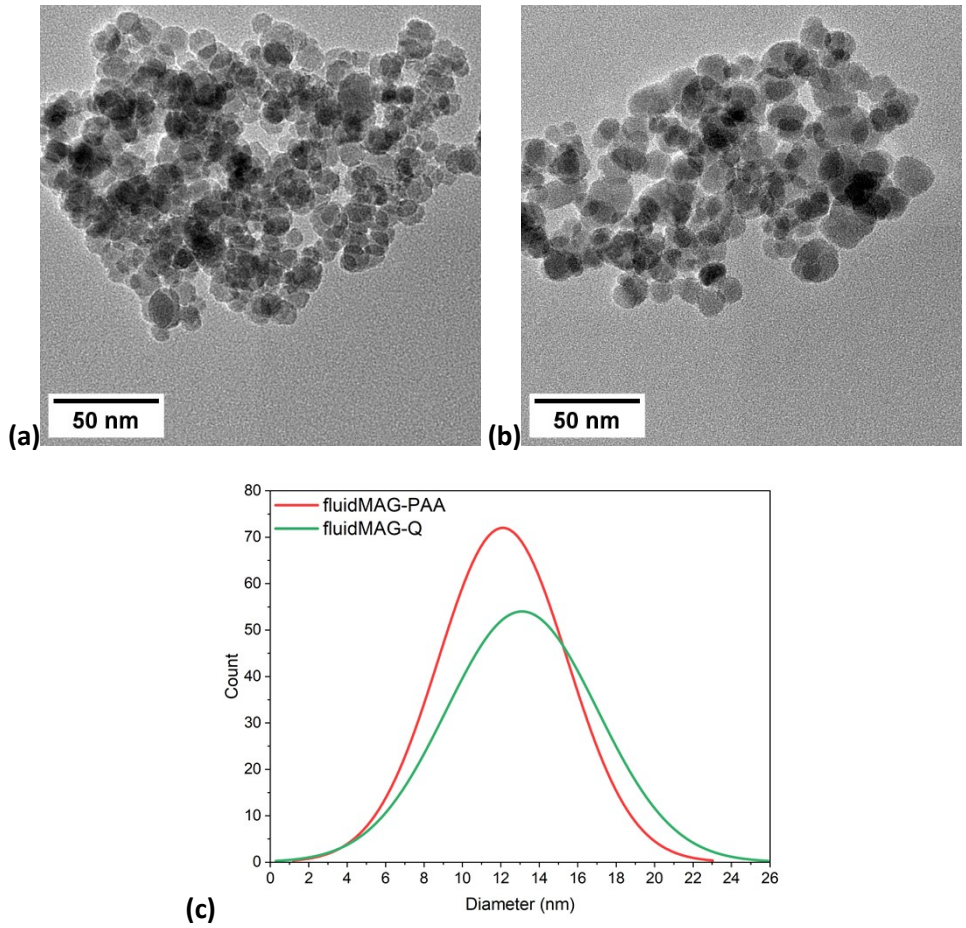

Figure S7. TEM images of **(a)** commercial PAA-coated maghemite nanoparticles (fluidMAG-PAA) and **(b)** PDADMAC-coated nanoparticles (fluidMAG-Q). (c) TEM diameter distribution of fluidMAG-PAA and fluidMAG-Q**.**

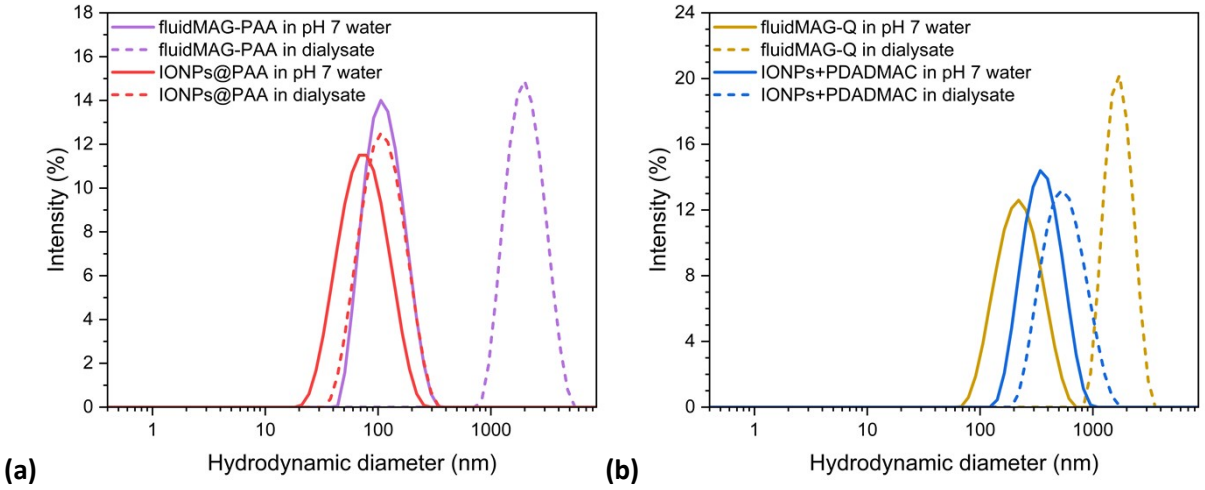

Figure S8. Hydrodynamic diameter distribution in pH 7 water and dialysate of **(a)** our own and commercial ("fluidMAG-PAA") PAA-coated nanoparticles and **(b)** our own and commercial ("fluidMAG-Q") PDADMAC-coated nanoparticles.

References

(1) Daou, T. J.; Pourroy, G.; Greneche, J. M.; Bertin, A.; Felder-Flesch, D.; Begin-Colin, S. Water Soluble Dendronized Iron Oxide Nanoparticles. *Dalton Trans.* **2009**, No. 23, 4442. https://doi.org/10.1039/b823187g.

(2) Basly, B.; Felder-Flesch, D.; Perriat, P.; Billotey, C.; Taleb, J.; Pourroy, G.; Begin-Colin, S. Dendronized Iron Oxide Nanoparticles as Contrast Agents for MRI. *Chem. Commun.* **2010**, *46* (6), 985–987. https://doi.org/10.1039/B920348F.

(3) Daou, T. J.; Begin-Colin, S.; Grenèche, J. M.; Thomas, F.; Derory, A.; Bernhardt, P.; Legaré, P.; Pourroy, G. Phosphate Adsorption Properties of Magnetite-Based Nanoparticles. *Chem. Mater.* **2007**, *19* (18), 4494–4505. https://doi.org/10.1021/cm071046v.

(4) Begin-Colin, S.; Felder-Flesch, D. Functionalisation of Magnetic Iron Oxide Nanoparticles. In *Magnetic Nanoparticles*; CRC Press, 2012; pp 151–192. https://doi.org/10.1201/b11760.

(5) Wiśniewska, M.; Urban, T.; Grządka, E.; Zarko, V. I.; Gun'ko, V. M. Comparison of Adsorption Affinity of Polyacrylic Acid for Surfaces of Mixed Silica–Alumina. *Colloid Polym Sci* **2014**, *292* (3), 699–705. https://doi.org/10.1007/s00396-013-3103-x.

(6) Swift, T.; Swanson, L.; Geoghegan, M.; Rimmer, S. The pH-Responsive Behaviour of Poly(Acrylic Acid) in Aqueous Solution Is Dependent on Molar Mass. *Soft Matter* **2016**, *12* (9), 2542–2549. https://doi.org/10.1039/C5SM02693H.

(7) Weidman, J. L.; Mulvenna, R. A.; Boudouris, B. W.; Phillip, W. A. Unusually Stable Hysteresis in the pH-Response of Poly(Acrylic Acid) Brushes Confined within Nanoporous Block Polymer Thin Films. *J. Am. Chem. Soc.* **2016**, *138* (22), 7030–7039. https://doi.org/10.1021/jacs.6b01618.

(8) Dultz, S.; Mikutta, R.; Kara, S. N. M.; Woche, S. K.; Guggenberger, G. Effects of Solution Chemistry on Conformation of Self-Aggregated Tannic Acid Revealed by Laser Light Scattering. *Science of The Total Environment* **2021**, *754*, 142119. https://doi.org/10.1016/j.scitotenv.2020.142119.

(9) Vaz-Ramos, J.; Lucante, T.; Greneche, J.-M.; Leuvrey, C.; Papaefthymiou, V.; Zafeiratos, S.; Carton, A.; Bégin, D.; Le Calvé, S.; Bégin-Colin, S. Impact of Tannic Acid on Iron Oxide Nanoclusters Synthesized by a Polyol Solvothermal Method. *Colloids and Surfaces A: Physicochemical and Engineering Aspects* **2024**, *689*, 133658. https://doi.org/10.1016/j.colsurfa.2024.133658.

(10) Yu, J.; Wei, W.; Menyo, M. S.; Masic, A.; Waite, J. H.; Israelachvili, J. N. Adhesion of Mussel Foot Protein-3 to TiO_2 Surfaces: The Effect of pH. *Biomacromolecules* **2013**, *14* (4), 1072–1077. https://doi.org/10.1021/bm301908y.

(11) Pillar-Little, E. A.; Guzman, M. I. Oxidation of Substituted Catechols at the Air–Water Interface: Production of Carboxylic Acids, Quinones, and Polyphenols. *Environ. Sci. Technol.* **2017**, *51* (9), 4951–4959. https://doi.org/10.1021/acs.est.7b00232.

(12) Pinnataip, R.; Lee, B. P. Oxidation Chemistry of Catechol Utilized in Designing Stimuli-Responsive Adhesives and Antipathogenic Biomaterials. *ACS Omega* **2021**, *6* (8), 5113–5118. https://doi.org/10.1021/acsomega.1c00006.

(13) Shultz, M. D.; Reveles, J. U.; Khanna, S. N.; Carpenter, E. E. Reactive Nature of Dopamine as a Surface Functionalization Agent in Iron Oxide Nanoparticles. *J. Am. Chem. Soc.* **2007**, *129* (9), 2482–2487. https://doi.org/10.1021/ja0651963.

(14) Kim, H.; Kim, H.; Kim, S. H.; Park, J. M.; Jung, Y. J.; Kwak, S. K.; Park, J. Molecularly Smooth and Conformal Nanocoating by Amine-Mediated Redox Modulation of Catechol. *Chem. Mater.* **2021**, *33* (3), 952–965. https://doi.org/10.1021/acs.chemmater.0c04068.

(15) Amstad, E.; Gillich, T.; Bilecka, I.; Textor, M.; Reimhult, E. Ultrastable Iron Oxide Nanoparticle Colloidal Suspensions Using Dispersants with Catechol-Derived Anchor Groups. *Nano Lett.* **2009**, *9* (12), 4042–4048. https://doi.org/10.1021/nl902212q.

(16) Narkar, A. R.; Barker, B.; Clisch, M.; Jiang, J.; Lee, B. P. pH Responsive and Oxidation Resistant Wet Adhesive Based on Reversible Catechol–Boronate Complexation. *Chem. Mater.* **2016**, *28* (15), 5432–5439. https://doi.org/10.1021/acs.chemmater.6b01851.

(17) Oćwieja, M.; Adamczyk, Z.; Morga, M. Adsorption of Tannic Acid on Polyelectrolyte Monolayers Determined in Situ by Streaming Potential Measurements. *Journal of Colloid and Interface Science* **2015**, *438*, 249–258. https://doi.org/10.1016/j.jcis.2014.09.071.
(18) Amstad, E.; Gehring, A. U.; Fischer, H.; Nagaiyanallur, V. V.; Hähner, G.; Textor, M.; Reimhult, E. Influence of Electronegative Substituents on the Binding Affinity of Catechol-Derived Anchors to Fe_3 O_4 Nanoparticles. *J. Phys. Chem. C* **2011**, *115* (3), 683–691. https://doi.org/10.1021/jp1109306.
(19) Yuen, A. K. L.; Hutton, G. A.; Masters, A. F.; Maschmeyer, T. The Interplay of Catechol Ligands with Nanoparticulate Iron Oxides. *Dalton Trans.* **2012**, *41* (9), 2545. https://doi.org/10.1039/c2dt11864e.
(20) Kim, H.; Woo, S.; Jung, H.; Ahn, H.-S.; Chen, N.; Cho, H.; Park, J. Amine-Assisted Catechol-Based Nanocoating on Ultrasmall Iron Oxide Nanoparticles for High-Resolution T_1 Angiography. *Nanoscale Adv.* **2023**, *5* (12), 3368–3375. https://doi.org/10.1039/D2NA00861K.
(21) Yeap, S. P.; Tia, S. Y. Induced Rapid Magnetic Sedimentation of Stabilized-Fe3O4 Nanoparticles by Bridging and Depletion Flocculation. *Chemical Engineering Research and Design* **2019**, *142*, 53–61. https://doi.org/10.1016/j.cherd.2018.12.004.
(22) Nedylakova, M.; Medinger, J.; Mirabello, G.; Lattuada, M. Iron Oxide Magnetic Aggregates: Aspects of Synthesis, Computational Approaches and Applications. *Advances in Colloid and Interface Science* **2024**, *323*, 103056. https://doi.org/10.1016/j.cis.2023.103056.
(23) Rosensweig, R. E. *Ferrohydrodynamics*; Courier Corporation, 2013.
(24) Daou, T. J.; Grenèche, J. M.; Pourroy, G.; Buathong, S.; Derory, A.; Ulhaq-Bouillet, C.; Donnio, B.; Guillon, D.; Begin-Colin, S. Coupling Agent Effect on Magnetic Properties of Functionalized Magnetite-Based Nanoparticles. *Chem. Mater.* **2008**, *20* (18), 5869–5875. https://doi.org/10.1021/cm801405n.
(25) Baaziz, W.; Pichon, B. P.; Fleutot, S.; Liu, Y.; Lefevre, C.; Greneche, J.-M.; Toumi, M.; Mhiri, T.; Begin-Colin, S. Magnetic Iron Oxide Nanoparticles: Reproducible Tuning of the Size and Nanosized-Dependent Composition, Defects, and Spin Canting. *J. Phys. Chem. C* **2014**, *118* (7), 3795–3810. https://doi.org/10.1021/jp411481p.
(26) Sanchez, L. M.; Martin, D. A.; Alvarez, V. A.; Gonzalez, J. S. Polyacrylic Acid-Coated Iron Oxide Magnetic Nanoparticles: The Polymer Molecular Weight Influence. *Colloids and Surfaces A: Physicochemical and Engineering Aspects* **2018**, *543*, 28–37. https://doi.org/10.1016/j.colsurfa.2018.01.050.
(27) Dong, J.; Ozaki, Y.; Nakashima, K. Infrared, Raman, and Near-Infrared Spectroscopic Evidence for the Coexistence of Various Hydrogen-Bond Forms in Poly(Acrylic Acid). *Macromolecules* **1997**, *30* (4), 1111–1117. https://doi.org/10.1021/ma960693x.
(28) Perton, F.; Cotin, G.; Kiefer, C.; Strub, J.-M.; Cianferani, S.; Greneche, J.-M.; Parizel, N.; Heinrich, B.; Pichon, B.; Mertz, D.; Begin-Colin, S. Iron Stearate Structures: An Original Tool for Nanoparticles Design. *Inorg. Chem.* **2021**, *60* (16), 12445–12456. https://doi.org/10.1021/acs.inorgchem.1c01689.
(29) Jones, F.; Farrow, J. B.; van Bronswijk, W. An Infrared Study of a Polyacrylate Flocculant Adsorbed on Hematite. *Langmuir* **1998**, *14* (22), 6512–6517. https://doi.org/10.1021/la971126l.
(30) Nadejde, C.; Neamtu, M.; Hodoroaba, V.-D.; Schneider, R. J.; Paul, A.; Ababei, G.; Panne, U. Tannic Acid- and Natural Organic Matter-Coated Magnetite as Green Fenton-like Catalysts for the Removal of Water Pollutants. *J Nanopart Res* **2015**, *17* (12), 476. https://doi.org/10.1007/s11051-015-3290-0.
(31) Falcão, L.; Araújo, M. E. M. Application of ATR–FTIR Spectroscopy to the Analysis of Tannins in Historic Leathers: The Case Study of the Upholstery from the 19th Century Portuguese Royal Train. *Vibrational Spectroscopy* **2014**, *74*, 98–103. https://doi.org/10.1016/j.vibspec.2014.08.001.
(32) Espina, A.; Sanchez-Cortes, S.; Jurašeková, Z. Vibrational Study (Raman, SERS, and IR) of Plant Gallnut Polyphenols Related to the Fabrication of Iron Gall Inks. *Molecules* **2022**, *27* (1), 279. https://doi.org/10.3390/molecules27010279.

(33) Roonasi, P. Adsorption and Surface Reaction Properties of Synthesized Magnetite Nano-Particles, 2007, 49.
(34) Andrade, Â. L.; Fabris, J. D.; Ardisson, J. D.; Valente, M. A.; Ferreira, J. M. F. Effect of Tetramethylammonium Hydroxide on Nucleation, Surface Modification and Growth of Magnetic Nanoparticles. *Journal of Nanomaterials* **2012**, *2012* (1), 454759. https://doi.org/10.1155/2012/454759.
(35) Padhye, L.; Luzinova, Y.; Cho, M.; Mizaikoff, B.; Kim, J.-H.; Huang, C.-H. PolyDADMAC and Dimethylamine as Precursors of *N* -Nitrosodimethylamine during Ozonation: Reaction Kinetics and Mechanisms. *Environ. Sci. Technol.* **2011**, *45* (10), 4353–4359. https://doi.org/10.1021/es104255e.
(36) Girase, C. D.; Rajput, Y. N.; Hatkar, V. M.; Kulkarni, R. D. Synthesis and Characterizations of Cationic Poly(DADMAC-Co-AM) Surfactant for Hair Care Applications. *J Polym Res* **2022**, *29* (8), 346. https://doi.org/10.1007/s10965-022-03113-3.
(37) *Chemistry and Properties of Biomolecular Systems*; Rizzarelli, E., Theophanides, T., Eds.; Lipscomb, W. N., Series Ed.; Topics in Molecular Organization and Engineering; Springer Netherlands: Dordrecht, 1991; Vol. 8. https://doi.org/10.1007/978-94-011-3620-4.
(38) McNeill, I. C.; Sadeghi, S. M. T. Thermal Stability and Degradation Mechanisms of Poly(Acrylic Acid) and Its Salts: Part 1—Poly(Acrylic Acid). *Polymer Degradation and Stability* **1990**, *29* (2), 233–246. https://doi.org/10.1016/0141-3910(90)90034-5.
(39) Hayashi, K.; Tomonaga, H.; Matsuyama, T.; Ida, J. Facile Synthesis, Characterization of Various Polymer Immobilized on Magnetite Nanoparticles Applying the Coprecipitation Method. *J of Applied Polymer Sci* **2022**, *139* (5), 51581. https://doi.org/10.1002/app.51581.
(40) Nahar, Y.; Rahman, M. A.; Hossain, M. K.; Sharafat, M. K.; Karim, M. R.; Elaissari, A.; Ochiai, B.; Ahmad, H.; Rahman, M. M. A Facile One-Pot Synthesis of Poly(Acrylic Acid)-Functionalized Magnetic Iron Oxide Nanoparticles for Suppressing Reactive Oxygen Species Generation and Adsorption of Biocatalyst. *Mater. Res. Express* **2020**, *7* (1), 016102. https://doi.org/10.1088/2053-1591/ab5be1.
(41) Francis, S.; Varshney, L.; Sabharwal, S. Thermal Degradation Behavior of Radiation Synthesized Polydiallyldimethylammonium Chloride. *European Polymer Journal* **2007**, *43* (6), 2525–2531. https://doi.org/10.1016/j.eurpolymj.2007.03.009.